

## Asymmetric Rotor Design for Synchronous Motor to Reduce Harmonics of Induced Voltage under Load Condition

Myung-Seop Lim<sup>1</sup>, Jae-Woo Jung<sup>2</sup>, Myung-Hwan Yoon<sup>3</sup>, Kyung-Tae Jung<sup>4</sup>, and Jung-Pyo Hong<sup>4\*</sup>

<sup>1</sup>School of Mechanical Engineering, Yeungnam University, Gyeongsbuk 38541, Korea

<sup>2</sup>R&D Center, Hyundai Mobis, Yongin 16891, Korea

<sup>3</sup>Hyundai Motor Company, Hwaseong 18280, Korea

<sup>4</sup>Department of Automotive Engineering, Hanyang University, Seoul 04763, Korea

(Received 4 June 2018, Received in final form 27 August 2018, Accepted 28 August 2018)

The harmonics of the induced voltage under load conditions cause the deterioration of the motor performance. It occurs when the peak value of the demand voltage exceeds the DC link voltage. In this paper, thus, to reduce the induced voltage harmonics under load conditions, an asymmetric rotor design method using the advanced inverse cosine function (AICF) is proposed. Using this method, the rotor shape is determined by considering the armature reaction under certain load condition. As a result, an improved concentrated flux synchronous motor (CFSM) achieving the required performance is designed. Lastly, the induced voltages waveforms of the proposed motors under the load conditions are compared through finite-element analysis (FEA) as well as experiments.

**Keywords :** Advanced inverse cosine function (AICF), asymmetric rotor, induced voltage, synchronous motor, voltage harmonics

### 1. Introduction

A variety of electrical motors are used for industrial equipment, medical equipment, home appliances, automobile parts, robots, etc. Especially, they have become essential components of vehicles as many automobile parts are applying electrical equipment. The harmonics of the induced voltage, however, has become a new issue as the usage of synchronous motors has increased in the automobile field [1, 2]. This is because the motors for automotive applications have high power density due to their space and weight limitations. In addition, this issue is becoming increasingly important because the motors of automobiles should be able to operate under the voltage limitation due to the battery usage in vehicles. If the peak value of the induced voltage under load conditions is partially higher than the DC link voltage as shown in Fig. 1, the inverter cannot apply the demand magnitude or waveform of the current to the armature coil. Therefore, the actual performance of the motor will decline com-

pared to the predicted performance [3-5]. This is because only the fundamental harmonic is considered for the d, q-axis equivalent circuit of the electric motors, which is generally used to predict the performance of the motors. Consequently, if the harmonic components of the induced voltage are not considered in the design method, the required speed or torque performance cannot be achieved.

In this paper, an asymmetric rotor design method for the synchronous motor using the advanced inverse cosine

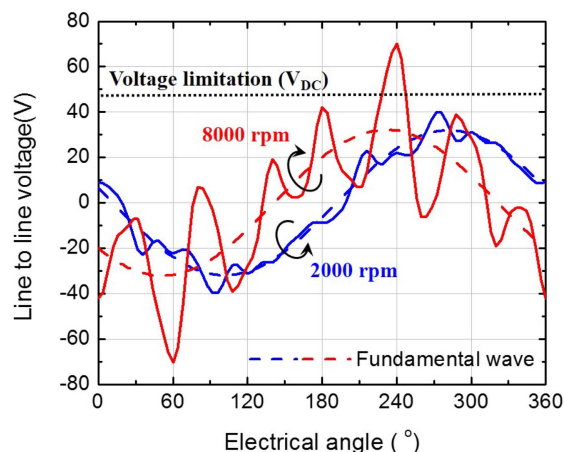


Fig. 1. (Color online) Induced voltages at 2000 and 8000 rpm.

function (AICF) is proposed. This is a novel design method that can achieve sinusoidal flux linkage and inductance waveforms at the air gap under a specific load condition considering the operation point of the machine. Therefore, the reference motor with a cylindrical rotor shape and the improved motor with an asymmetric rotor shape designed by using AICF are proposed. Finally, the induced voltage of the improved motor will be compared with that of the reference motor to verify the analysis and design methods. Consequently, it is inferred that the machine performance is not deteriorated because the peak value of the demand voltage does not exceed the DC link voltage due to the proposed design method using AICF.

## 2. Design Method Using Advanced Inverse Cosine Function (AICF)

A new design method is proposed herein to reduce the harmonics of the induced voltage under the load condition. Therefore, AICF as the new function is derived and proposed to make the sinusoidal air gap flux density considering the operating point of the motor.

AICF is an equation that adjusts the air gap length by considering the effect of the armature reaction. For the convenience of the analytical approach, the permeability of the magnetic core is assumed to be infinite. In addition, it is assumed that the magneto-motive force (MMF) distribution by the armature winding can be considered sinusoidal because only the fundamental component of the armature MMF is considered in this study, regardless of the winding method. Figure 2 is a simplified representation of the air gap MMF by the PM as well as armature winding under load conditions. In Fig. 3, the red line with the square symbol as the total air gap MMF is the sum of the MMFs by the PM and armature winding shown in Fig. 2. Consequently, the armature reaction causes a decrease in the total air gap flux density under

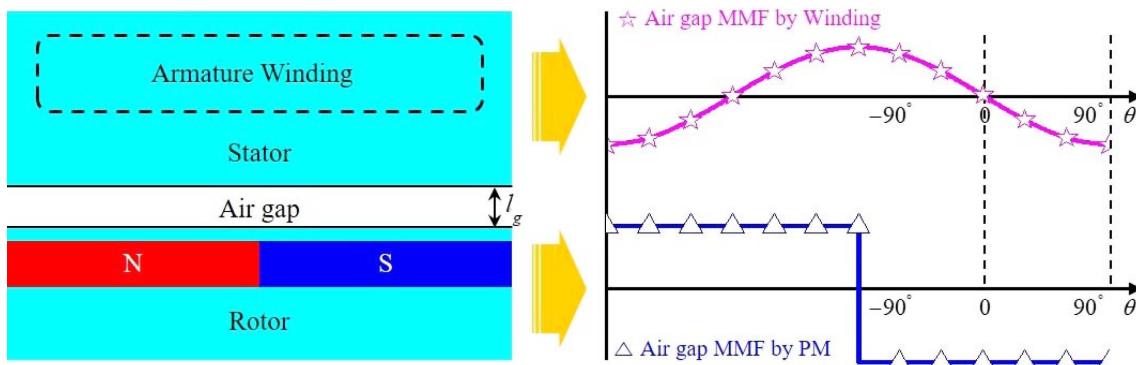


Fig. 2. (Color online) Air gap MMF distribution by armature winding and PM.

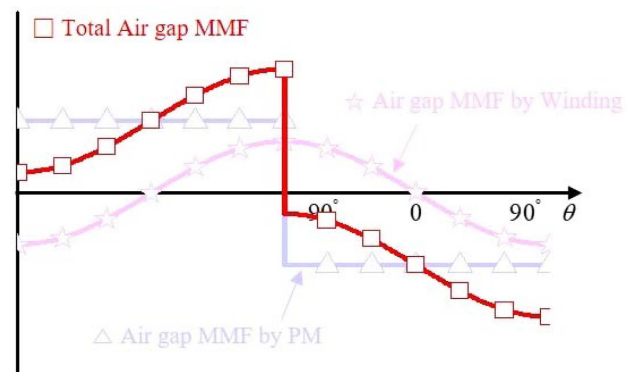


Fig. 3. (Color online) Total air gap MMF distribution considering armature reaction.

one half of the pole, and an increase under the other half. AICF enlarges the air gap length of the area where the air gap flux density is increased by the armature reaction. On the other hand, it reduces the air gap length of the area where the flux density is declined by the armature reaction. Therefore, through the uneven air gap length, the air gap flux density distribution is rendered sinusoidal, as shown in Fig. 4.

The air gap flux density of motors can be described as the periodic function of (1) according to angle  $\theta$ .

$$B_{\max} \cos \theta = \frac{\mu_0 F_g}{l_g(\theta)}, \quad (1)$$

where  $l_g(\theta)$  is the air gap length by  $\theta$ ,  $\mu_0$  is the permeability of the vacuum,  $F_g$  is the air gap MMF,  $B_{\max}$  is the maximum value of the air gap flux density, and  $\theta$  varies from  $-90^\circ$  to  $+90^\circ$  in the electrical angle. As can be seen in Fig. 4, the total air gap MMF can be expressed as (2) measured from the center of the  $N$  pole.

$$F_g = F_m - F_w \sin(\theta + \beta), \quad (2)$$

where  $F_m$  is the air gap MMF of the PM,  $F_w$  is the air gap

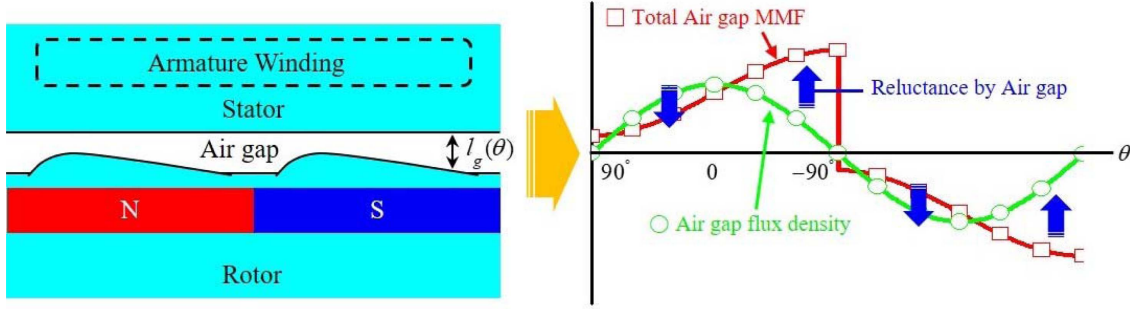


Fig. 4. (Color online) Air gap MMF and flux density considering armature reaction.

MMF of the armature current, and  $\beta$  is the current phase angle. Hence, equations (3)-(5) are generated by substituting (2) into (1).

$$l_g(\theta) = \frac{l_{\min}}{\cos \theta} - k_F \frac{l_{\min} \sin(\theta + \beta)}{\cos \theta}, \quad (3)$$

where

$$l_{\min} = \frac{\mu_0 F_m}{B_{\max}} \quad (4)$$

$$k_F = \frac{F_w}{F_m}, \quad (5)$$

where  $l_{\min}$ , is the minimum value of the air gap length. As an example, for the maximum air gap flux density on the  $d$ -axis position, if the flux density is sinusoidal, the  $d$ -axis air gap length can be  $l_{\min}$ . The first term on the right side of (3) is the air gap length derived from the inverse cosine function (ICF), and the second term is added considering the effect of the armature reaction through the proposed AICF [6, 7]. As can be seen in (3),  $k_F$  is an important factor that determines the asymmetric shape of the AICF model and is defined as the ratio of the air gap MMF due to the PM to the air gap MMF provided by the armature reaction. As  $k_F$  increases, the shape of the rotor becomes more asymmetric.

To determine  $k_F$ ,  $F_m$  and  $F_w$  should be calculated.  $F_m$  can be calculated using the equivalent magnetic circuit, which is shown in Fig. 5.  $F_r$  and  $R_m$  are the equivalent MMF and the equivalent reluctance of the PM, and  $R_g$  is the air gap reluctance.  $F_r$  can be calculated using equation (6).  $F_m$  can be calculated using equation (7), according to the equivalent magnetic circuit, and  $F_w$  can be calculated using equation (8).

$$F_r = \frac{B_r l_m}{\mu_0} \quad (6)$$

$$F_m = \frac{F_r}{R_m + R_g} R_g \quad (7)$$

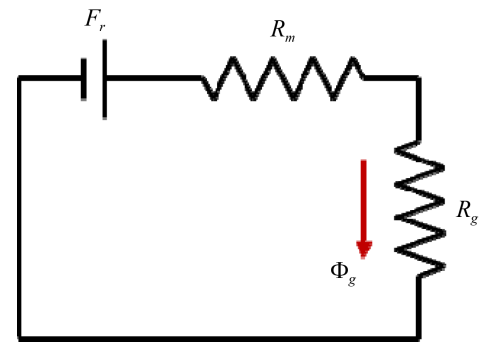


Fig. 5. (Color online) Equivalent magnetic circuit of the permanent magnet motors.

$$F_w = 1.5 k_w \frac{\sqrt{2} N_{ph} I_{rms}}{2pp}, \quad (8)$$

where  $F_r$  and  $F_m$  are the MMF source produced by the PM and the MMF of the PM at the air gap, respectively;  $F_w$  is the MMF of the armature winding at the air gap;  $B_r$  is the residual induction;  $l_m$  is the thickness of the PM;  $R_m$  is the internal reluctance of the PM;  $k_w$  is the winding factor;  $N_{ph}$  is the series of turns per phase;  $I_{rms}$  is the  $rms$  current; and  $pp$  is the number of pole pairs.

The air gap length is the minimum length determined considering the mechanical stability and manufacturing tolerance. As shown in Fig. 6, however, the air gap length of the AICF model was partially decreased when AICF was applied using equation (3). Accordingly, offset  $\delta$  of

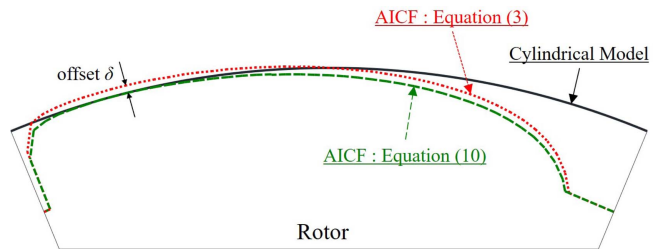


Fig. 6. (Color online) Rotor shape considering  $\delta$  offset.

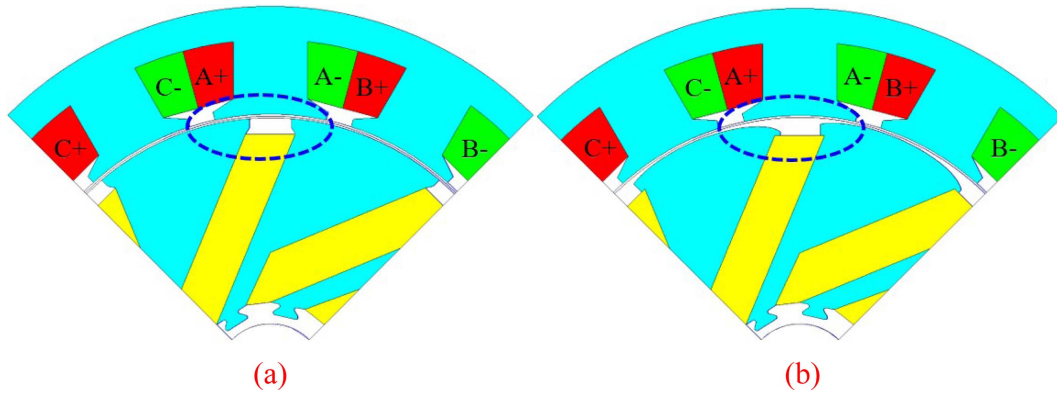


Fig. 7. (Color online) Shape of the motor (a) Reference motor: Cylindrical (b) Improved motor: AICF.

the rotor surface was applied to equation (3) for the modification of the minimum air gap length to secure mechanical stability. Offset magnitude  $\delta$  of the AICF model was determined to ensure that the minimum air gap length of the AICF model would be equal to the air gap length of the conventional cylindrical rotor shape model. Thus,  $\delta$  can be defined as equation (9).

$$\delta = l_{\min} - \text{minimum} \left( \frac{l_d}{\cos \theta} - k_F \frac{l_d \sin(\theta + \beta)}{\cos \theta} \right) \quad (9)$$

The modified air gap length was determined by offsetting the rotor surface in a radially inward direction by as much as  $\delta$  from the rotor shape of the AICF model calculated using equation (3). Consequently, equation (3) was modified to equation (10).

$$l_g(\theta) = \frac{l_{\min}}{\cos \theta} - k_F \frac{l_{\min} \sin(\theta + \beta)}{\cos \theta} + \delta \quad (10)$$

Figure 6 shows the difference in the rotor shapes using equations (3) and (10) as an example.

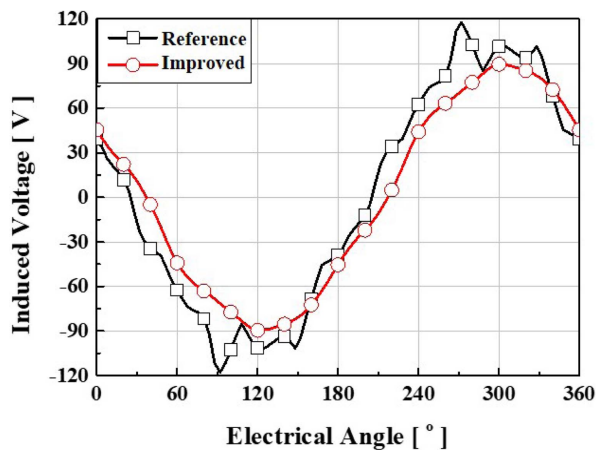


Fig. 8. (Color online) Induced voltage waveforms of reference and improved motor.

### 3. Verifications of the Proposed Design Method

#### 3.1. Analysis Model

In this paper, two analysis models are presented. The first one is the reference model having a cylindrical shape of rotor. The second one is the improved model having an asymmetric shape. The improved motor was designed based on AICF by using equation (10). Considering the 22 Nm at 3000 rpm load condition, which is the target operating point of the proposed motors,  $k_F$  was deter-

Table 1. Specifications of the proposed motors.

Quantity	Unit	Specification
DC voltage	V <sub>DC</sub>	280
Power	kW	6.9
Torque	Nm	22
Speed	rpm	3,000
Outer diameter	mm	170
Stack length	mm	135

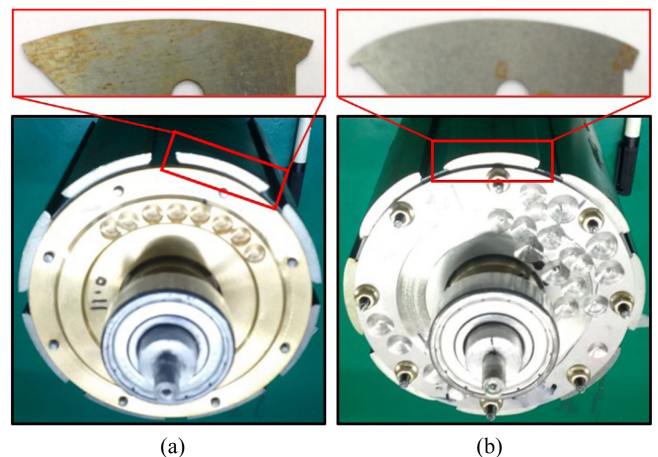


Fig. 9. (Color online) Manufactured rotor and core shape (a) Reference motor (b) Improved motor.

mined to be 0.90. In addition,  $\delta$  was calculated as 0.34 mm. The shapes, induced voltage waveforms, and specifications of the motors are shown in Fig. 7, Fig. 8, and Table 1, respectively. As shown in the Fig. 7, the reference motor has the cylindrical shape rotor, and the

improved motor has the asymmetric shape rotor.

### 3.2. Verification

To verify the proposed method, proposed motors are manufactured and experiments using the proposed motors were conducted under load conditions. The manufactured rotors and core shapes of the reference and improved motors are presented in Fig. 9, and Fig. 10 shows the experiment set for the load tests. The load test requires a driver, controller, dynamometer, power analyzer, oscilloscope, etc. For the test, the test motor is operated by the torque control and the load motor is operated by the speed control. Input voltage and current are measured by using voltage and current probes as well as oscilloscope, and input power is calculated through the power analyzer. Output power is calculated by measuring the torque and rotational speed. The test is conducted at two different operating points under the conditions of 16 Nm at 1500 rpm and 22 Nm at 3000 rpm. Figure 11 presents the

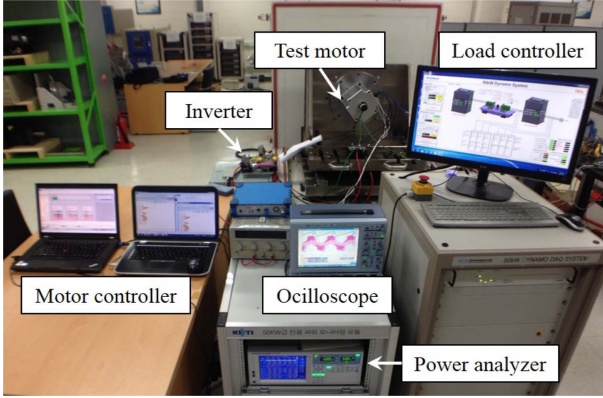


Fig. 10. (Color online) Experiment set for the load tests.

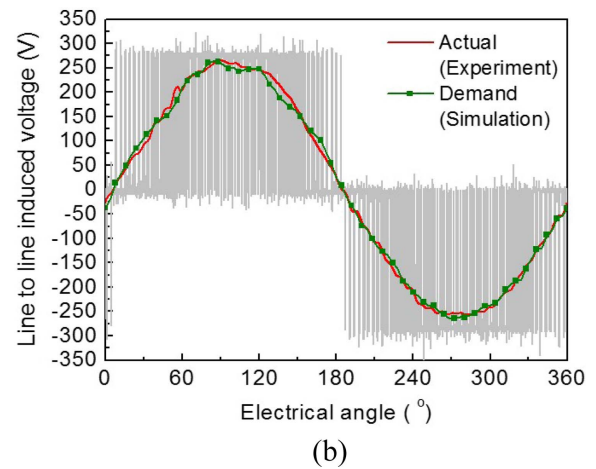
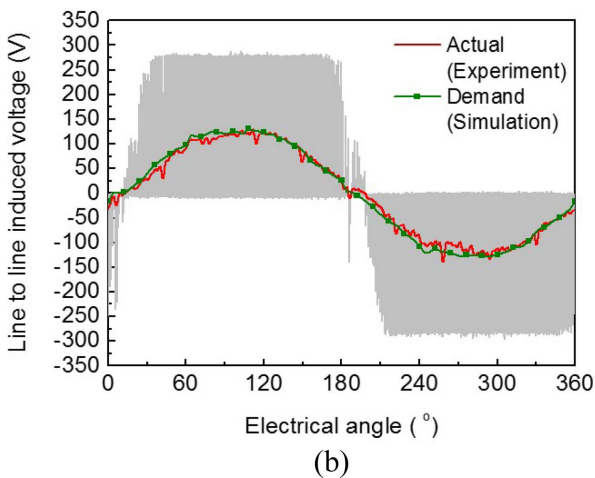
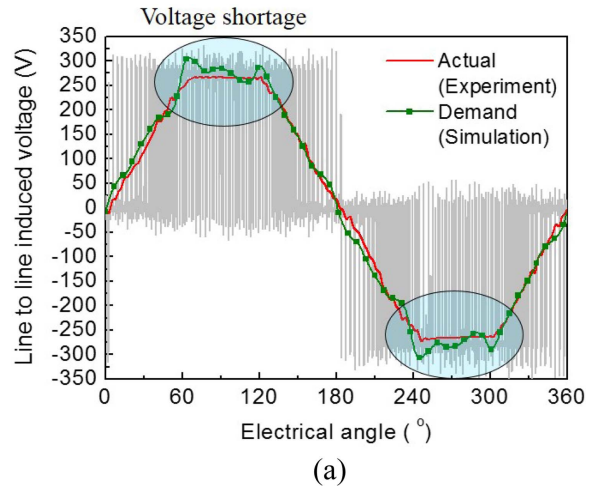
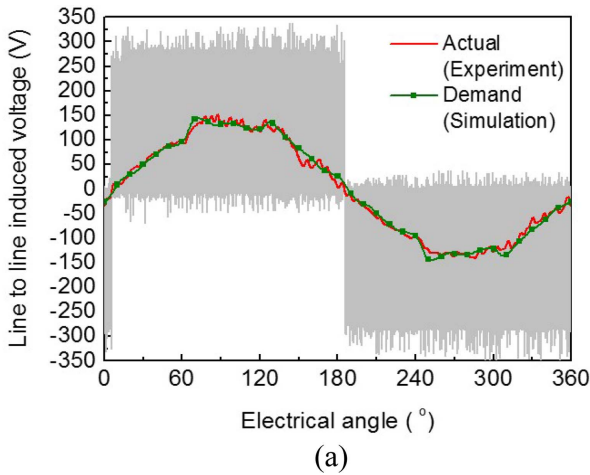


Fig. 11. (Color online) Induce voltage of the motors under 16 Nm at 1500 rpm condition (a) reference motor (b) improved motor.

Fig. 12. (Color online) Induce voltage of the motors under the target load condition of 22 Nm at 3000 rpm (a) reference motor (b) improved motor.

induced voltage waveforms of the proposed motors under the 16 Nm at 1500 rpm load condition obtained from the simulations and experiments. As shown by the results, the induced voltage in both motors did not exceed the voltage limitation. The voltage limitation was the value of the maximum line-to-line voltage calculated from the DC link voltage. On the other hand, given the results under the 22 Nm at 3000 rpm load condition, the actual operating point of the machine, the induced voltage of the reference motor obtained from the FEA obviously exceeds the voltage limitation, as shown in Fig. 12(a). The actual induced voltage obtained from the experiment, however, cannot exceed the voltage limitation physically. Consequently, the required current or sinusoidal current waveform cannot be applied to the reference motor to fulfill the required performance. Under the same load condition, however, the induced voltage of the improved motor does not exceed the voltage limitation, as shown in Fig. 12(b). As such, the required current can be applied to the motor, and the required performance can be achieved. It can be concluded that the demand current waveform for the reference motor cannot be applied at the operating point because of the induced voltage, contrary to the improved motor.

#### 4. Conclusion

As pointed out in the introduction, the harmonics of the

induced voltage cause the performance deterioration of the electric motors. Therefore, in this study, an asymmetric rotor design method using the AICF was proposed, and an improved motor was designed by using the ACIF. Given that the experimental results, the harmonic distortion of the induced voltage of the improved motor was lower than that of the reference motor. As such, the induced voltage of the improved motor does not exceed the voltage limitation, contrary to the reference motor. Consequently, it can be concluded that the proposed design method will be helpful in designing high-performance synchronous motors.

#### References

- [1] M. Chowdhury, A. Gebregergis, M. Islam, and T. Sebastian, *IEEE Int. Electric Machines and Drives Conf. (IEMDC)*, 260 (2013).
- [2] M. H. Yoon, D. Y. Kim, S. I. Kim, and J. P. Hong, *J. Magn.* **20**, 387 (2015).
- [3] W. Liang, J. Wang, P. C. K. Luk, W. Fang, and W. Fei, *IEEE Trans. Energy Conv.* **29**, 673 (2014).
- [4] J. C. Hwang, and H. T. Wei, *IEEE Trans. Power Electron.* **29**, 3032 (2014).
- [5] T. Hiraide, K. Abe, K. Ohishi, and H. Haga, *IEEE Trans. Industrial Electronics Conference (IECON)*, 2697 (2013).
- [6] S. A. Evans, *Int. Conf. Electric Machines*, 1 (2010).
- [7] K. Wang, Z. Q. Zhu, G. Ombach, and W. Chlebosz, *IEEE Trans. Ind. Electron.* **61**, 5047 (2014).